Journal of Power Sources 223 (2013) 325–335

Contents lists available at SciVerse ScienceDirect

Journal of Power Sources

journal homepage: www.elsevier.com/locate/jpowsour

Transient efficiency measurement of a combined heat and power fuel cell generator

Jenn-Jiang Hwang*

Department of Greenergy, National University of Tainan, Tainan, Taiwan

HIGHLIGHTS

- The instantaneous thermal efficiency and CHP efficiency reach as high as 60% and 81%, respectively.
- The power-conditioning system copes with the fast dynamics of variable loads.
- The electrical efficiency is as high as 40% under 55% system power loads.
- Average CHP efficiency is as high as 61% under 55% system power loads.

ARTICLE INFO

Article history:
Received 10 August 2012
Received in revised form
23 September 2012
Accepted 24 September 2012
Available online 1 October 2012

Keywords:
Combined heat and power
Fuel cell generator
Efficiency
Power conditioning system

ABSTRACT

The objective of the present paper is to conduct an experimental work to measure transient thermal/electrical efficiencies in a combined heat and power (CHP) fuel cell generator. An original-designed fuel cell CHP generator comprising a proton exchange membrane (PEM) fuel cell system, a power conditioning system, and a thermal recovery system is constructed. The thermal recovery system recaptures the thermal energy dissipated by the fuel cell stack, while the power conditioning system distributes the electrical power of the fuel cell system. Performance matrices including stack electrical efficiency, system electrical efficiency, thermal efficiency, and CHP efficiency are presented. Particular attention is placed on the variation of transient system efficiencies as the load is changed drastically. The time-averaged system efficiency is then concluded from the statistics of the transient system efficiency. Results show that the time-averaged efficiencies in electrical, thermal and CHP are about 37%, 24%, and 61%, respectively, under 55% electrical power capacity of the generator. The instantaneous CHP efficiency could reach as high as 85% in the loading period.

1. Introduction

Combined heat and power (CHP), also known as cogeneration, is the simultaneous production of electrical energy (power) and useful thermal energy (heat) from a single energy stream such as natural gas [1]. There is a growing potential for the use of micro-CHP systems in the residential sector and small-scale commercial applications like hotels, hospitals, marketplace, or institutional buildings. Their use aims to meet the electrical and thermal demands of a building for space and domestic hot water heating and, possibly, absorption cooling. The efficiency of energy conversion of a CHP system could increase to over 80%, which is higher than the combined ones that heat and electricity are generated independently by using conventional methods. The higher energy efficiency could result in lower costs and reduction in greenhouse gas (GHG) emissions.

Fuel cell technology is an emerging technology with a potential for both electricity generation and CHP applications with performance advantages and in an environmentally friendly fashion [2–6]. The advantages of fuel cell CHP generators include low noise level, potential for low maintenance, low emissions, and high overall efficiency even with small units. Stationary fuel cell CHP generators typically run with natural gas, and release fewer environmentally harmful emissions than those produced by combustion CHP plants. Low emissions and noise levels make fuel cell CHP systems particularly suitable for residential, commercial and institutional applications. Among varied types of fuel cells, proton exchange membrane (PEM) fuel cells are regarded as the lead for residential CHP application because of good match in thermal/electric power ratios [7–9]. Actually, PEM fuel cell based residential CHP systems has been reaching commercial stages. Japan's ENE-FARM scheme, the joint home use fuel cell marketing brand of

* Tel./fax: +886 62602251.
E-mail address: azaijj@mail.nutn.edu.tw.

0378-7753/$ – see front matter © 2012 Elsevier B.V. All rights reserved.
http://dx.doi.org/10.1016/j.jpowsour.2012.09.086

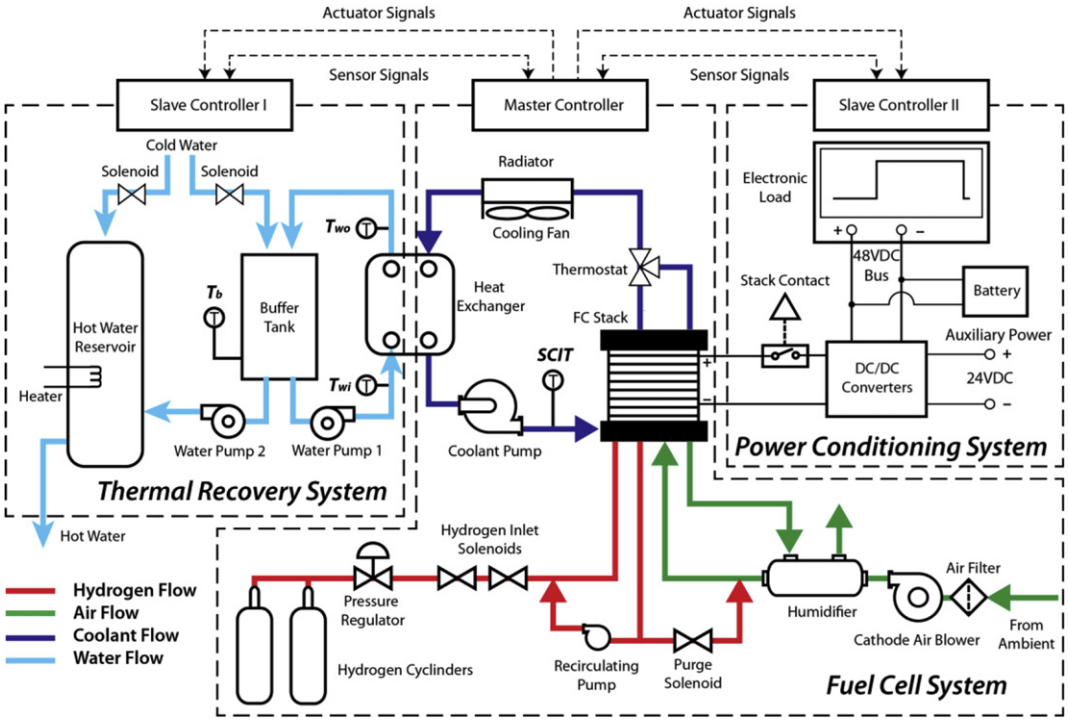

Fig. 1. Schematic drawing of the fuel cell CHP generator.

several major gas companies and fuel cell manufacturers, has seen consistent success since its launch in 2005, particularly after a government subsidy scheme was introduced [10,11]. Each model of ENE FARM, whose rated power is from 0.7 to 1 kW, generates power and hot water for domestic use efficiently with electrical efficiency of over 35% and overall efficiency of over 80% [12–14]. With the high performance, large reduction in primary energy consumption is expected. In addition to PEM fuel cells, solid oxide fuel cells (SOFCs) are being introduced to residential CHP schemes in the ENE FARM program [15]. In general, SOFCs run efficiently at high temperatures and also have a favorable thermal/electric ratio [9,16]. In addition, they are more tolerant of carbon monoxide in the fuel and this allows for some simplification of the system configuration. However, many other problems may be present such as start-up or load following constraints [17].

In the past decade, quite a few modeling and experimental research efforts related to the fuel cell CHP system have been carried out [18–27]. Most of the experimental works are related to the time-averaged characteristics in a fuel cell CHP system. The experimental results of transient thermal/electrical efficiencies in a PEM fuel cell CHP system is relatively sparse, especially in the conditions of highly variant loads. This motivates the present work to conduct an experimental work to realize the transient thermal/electrical characteristics in a fuel cell CHP system. Focus is particularly placed on the transient dynamic results in the severe conditions of high load variations. First, a PEM fuel cell system, a power conditioning system, and a thermal recovery system are designed, fabricated, and tested to verify their availability. Then, they are integrated into a fuel cell CHP generator. Subsequently, smart control algorithms burning into the controllers are employed to control the fuel cell CHP system both electrically and thermally. Successively, checking the electrical and thermal dynamic behaviors assesses the performances of the fuel cell CHP generator. The dynamics of thermal and electrical properties such as voltage, current, power, and temperature are measured to prove the stability of the fuel cell CHP generator. Moreover, the transient dynamics of system efficiencies, including electrical efficiency, thermal efficiency, and combined heat and power efficiency, are further determined under step-changed external loads and discussed thereafter. Finally, the average system efficiency is concluded from the statistics of the transient system efficiency.

2. Experimental setup

2.1. Fuel cell system

Fig. 1 gives a schematic drawing of the fuel cell CHP generator. It comprises a PEM fuel cell system producing electrical energy, a thermal recovery system recovering the thermal energy dissipated by the fuel cell stack, and a power condition system interconnecting the power sources and the external loads.

The fuel cell system is equipped with a 4-kW PEM fuel cell stack, which serves as the major power source of the generator. The self-made stack has an active area of 225 cm^2 and connects 63 cells in

Table 1
Brief technical specifications of the fuel cell stack.

Specifications	Value
Number of cells	63
Active area	225 cm^2
Pt-loading, cathode	0.2 g cm^{-2}
Pt-loading, anode	0.15 g cm^{-3}
Bipolar plate material	Plastic-graphite composite
Flow-field type	Multiple serpentine channels
Membrane	Nafion® 117
Rated power	4000 W
Anode feeding	Gaseous hydrogen, 99.95% in purity
Cathode feeding	Ambient air
Cut-off voltage	40 V
Maximum power	5800 W
Operating voltage range	42–60 VDC
Operating current range	0–110 A

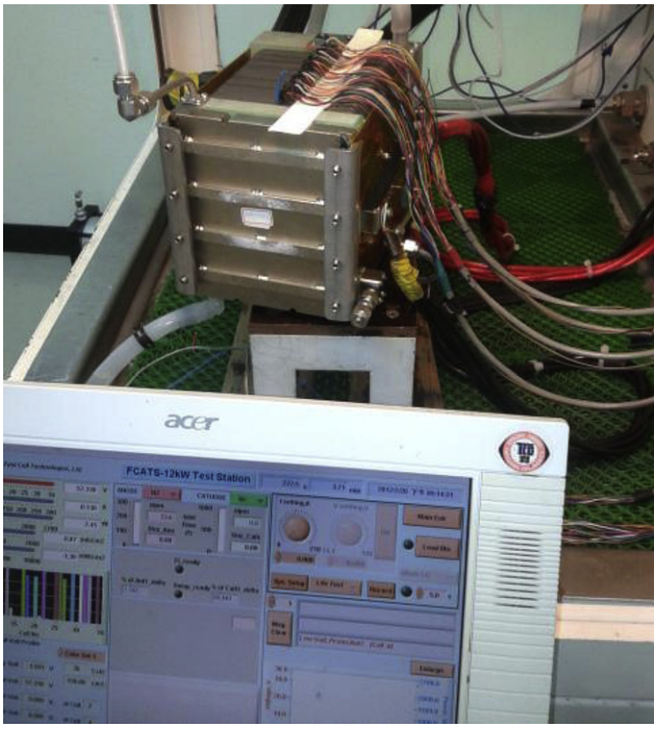

Fig. 2. Fuel cell system test with a man–machine interface.

series. The technical specifications of the stack are summarized in Table 1. A 24VDC brushless air blower supplies the stack cathode with air for electrochemical reduction reaction. It is filtered and humidified before entering the stack cathode. The airflow rate is a function of stack power, which is regulated by adjusting the speed of the blower. A hollow-fiber membrane humidifier transfers heat and humidity from the cathode outlet gases to the cathode inlet airstream. In the hydrogen delivery subsystem, pure hydrogen from the high-pressure cylinders feeds the stack anode for oxidation reaction. A hydrogen pump is employed to recirculate the unreacted hydrogen in the anode into the hydrogen pipeline at the stack anode inlet [28,29]. The bypass of the anode exhaust is equipped with a solenoid valve which conditionally purges exhausts and inert to the stack cathode inlet to burn them up. In general, the feeding of hydrogen depends on the hydrogen pressure in the anode. During operation, the hydrogen pressure in the stack anode decreases gradually due to the hydrogen oxidation reaction. When the anode hydrogen pressure is lower than a pre-set value, the solenoid valves on the hydrogen pipeline ahead of the stack opens to feed the anode with hydrogen and thus increases the hydrogen pressure. Then, the solenoid valves shut and the hydrogen pressure in the anode decreases due to the oxidation reaction again. Consequently, the solenoid valves are switched on/off again and again to maintain the anode hydrogen pressure in a proper range during operation. Depending on the requirements of duty cycles of the fuel cell CHP system, the solenoid valves selected here are very reliable (Mindman, MSUS series) [30] with durability over millions cycles in lifetime. As for the stack cooling, a coolant pump drives the coolant through the parallel cooling channels in the stack to

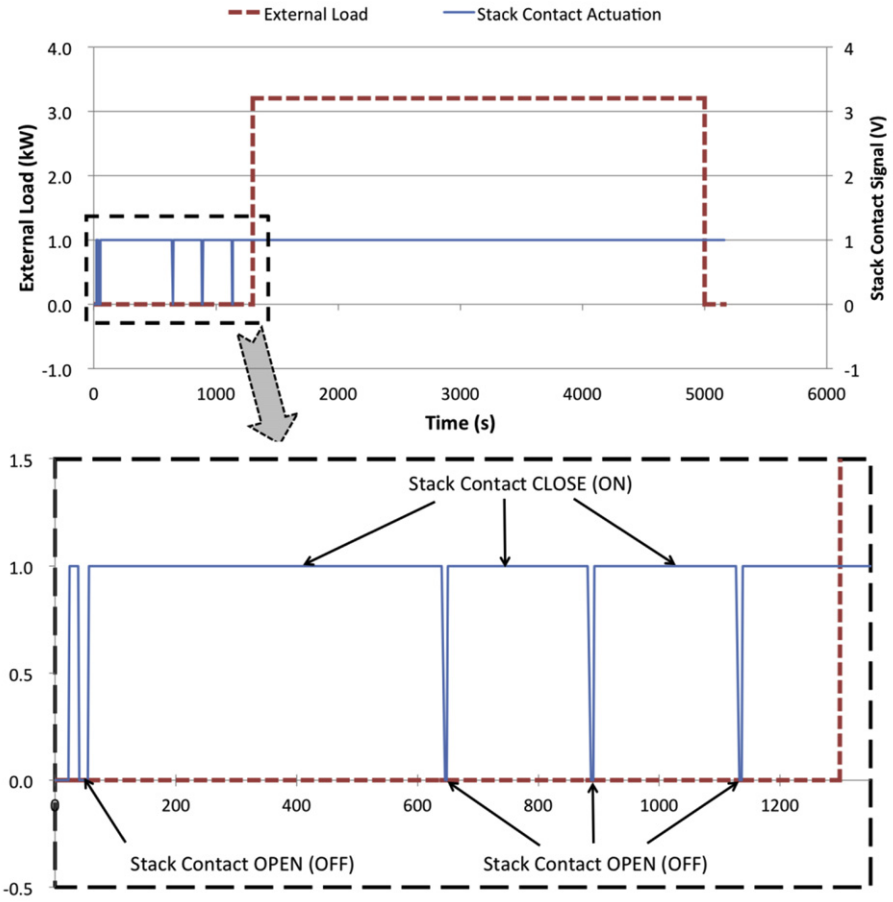

Fig. 3. External load profile and operation conditions of the present work.

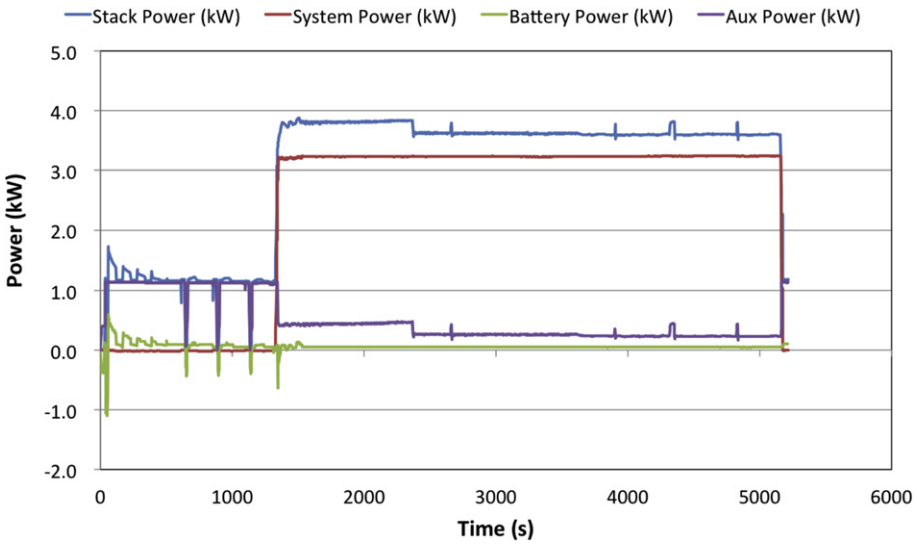

Fig. 4. Power dynamics of the fuel cell CHP generator under the external load profile of Fig. 3.

remove the heat dissipated by the stack. Then, the hot coolant from the stack outlet passes through a flat plate heat exchanger to discharge thermal energy to the cool water in the water circuit. A temperature sensor installed on the stack coolant circuit ahead of the stack monitors the stack coolant inlet temperature (SCIT), which serves as a control point for stack thermal stabilization. Note that there is an about 10 °C in thermal delay between the SCIT and the temperature inside the stack [31,32]. Therefore, the SCIT is controlled at 60 °C in the steady state, which ensures the fuel cell stack running with a temperature around 70 °C. The stack coolant used herein is a mixture of 50% glycol and 50% DI water, which has a specific thermal capacity of $C_p = 1.75$ kJ kg^{-1} K^{-1}.

2.2. Thermal recovery system

As shown Fig. 1, the thermal recovery system connects the cooling circuit of the fuel cell system by using a flat plate heat exchanger. The hot stack coolant in the cooling circuit (dark-blue lines) dumps its thermal energy to the cold water in the flat plate heat exchanger. A water pump P1 circulates the tap water from the buffer tank through the flat plate heat exchanger, and then back to the buffer tank. Two temperature sensors are installed at the entrance (T_{wi}) and the exit (T_{wo}) of the flat plate heat exchanger to measure the water temperature difference across the heat exchanger. A 50-gallon hot water reservoir is employed to store the thermal energy recovered by the hot water. Another water pump P2 pumps the hot water from the buffer tank to the hot-water reservoir when the water temperature in the buffer tank is getting higher than a pre-set value. The hot water reservoir is installed with an ancillary electrical heater to ensure sufficient hot water supply under low thermal/electric ratio conditions. In addition, a radiator together with a turbofan is installed in the stack coolant circuit. The radiator turbofan starts working to maintain fuel cell cooling instead of the heat removal by the heat exchanger as the hot-water reservoir is full. Note that as far as cost concerns, the present system is not optimized yet due to the need of both storage and radiator. Both the buffer tank and the hot water reservoir are equipped with a level sensor to maintain the water level.

2.3. Power conditioning system

The general function of the power conditioning system is providing a proper interface between the power sources and the external load. As shown in Fig. 1, major components of the power conditioning system include a bidirectional (boost/buck) DC–DC converter, a stack contact switch, a programmable electronic load, and a power controller. In addition, a lithium-ion battery of a nominal voltage of 48 VDC and a nominal capacity of 10 Ah is coupled with the fuel cell stack to provide quick-response power to variable loads. The bidirectional DC–DC converter is operated to distribute the power flow among the primary power, the auxiliary power, and the external load, which uses multiphase technique to generate PMW (pulse width modulation) signals to control the power flow. When the fuel cell stack is operating, the stack power is boosted to positive 48VDC by the converter for external load, and part power is bucked to positive 24VDC for the auxiliary power. As soon as the power deficiency/excess occurs due to load variations, the converter could regulate the power flow from/to the lithium-ion battery. For example, during the high power demand conditions, the converter boosts the stack power to the load and meanwhile the lithium-ion battery discharges to add extra power to the load. In contrast, when the stack power is larger than the power demand by the external load, the converter boosts the stack power to provide the power to the external load, and the extra stack power is used to charge the lithium-ion battery. In addition, during the startup instant, the slow dynamics of the fuel cell stack retards the power delivery; instead, the lithium-ion battery discharges the current to power the auxiliary components through the converter. Note also that a stack-contact switch is installed between the stack and the converter to protect the stack from any possible damages by accidents such as voltage shocks. As mentioned above, the need of battery in a fuel cell system is because it could take some of the peak power demands, thereby reducing the size of the fuel cell stack. Of most importance, it copes with the rapid dynamics of variable loads and allows extra energy storage. According to author's experience [29], the fuel cell system without battery to propel an electrical vehicle would cause stack damages easily due to the slower dynamics of the fuel cell as compared to those of the electrical motor.

2.4. Control system

As shown in Fig. 1, the control system of the generator includes a master controller for the fuel cell system and two slave controllers for the thermal recovery system and the power conditioning system, respectively. It is designed for safe and autonomous operation and

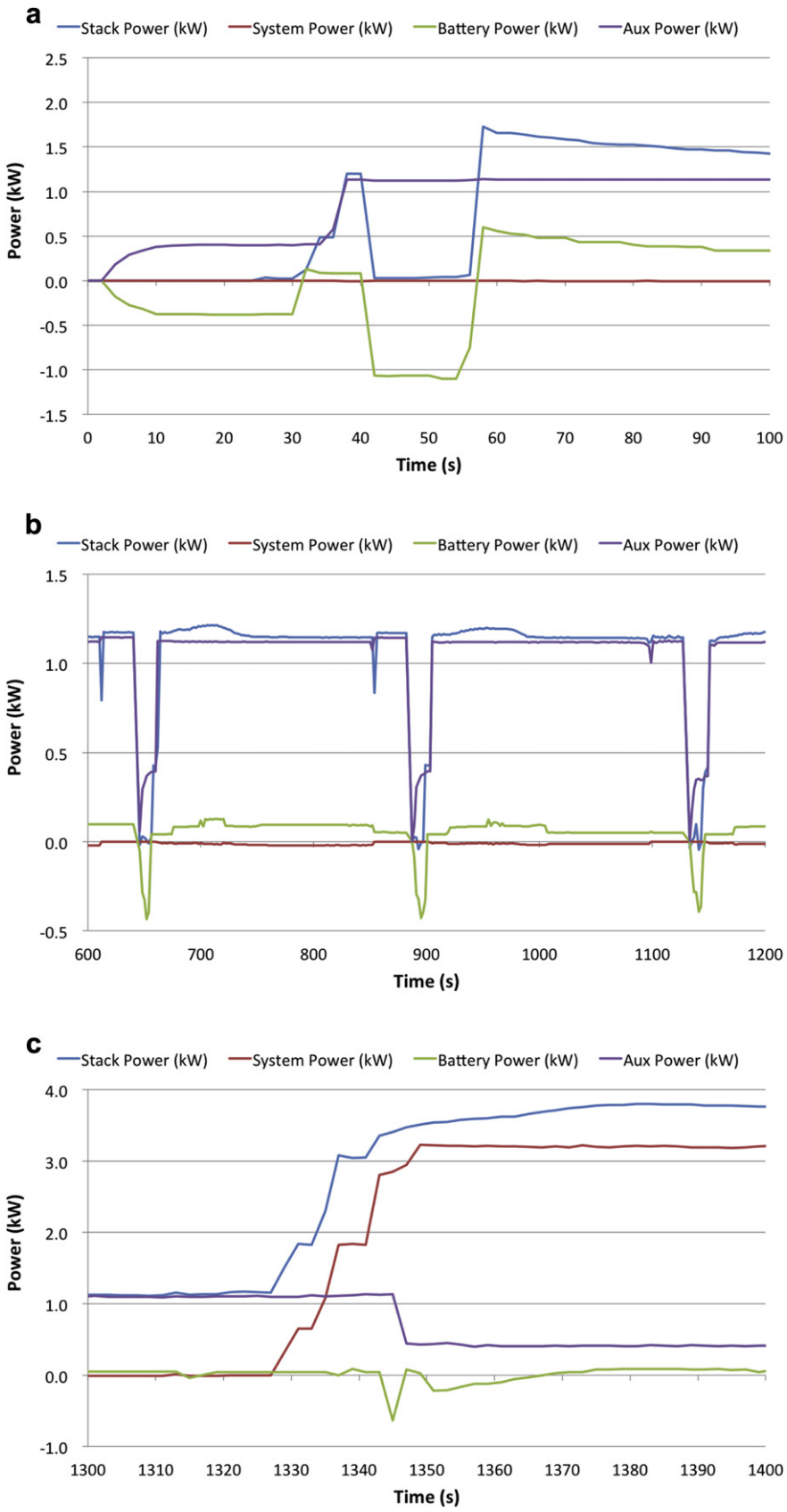

Fig. 5. (a) Local magnification of Fig. 3 in the system startup period, $0 < t < 100$ s. (b) Local magnification of Fig. 3 in the stack contact switching period, $600\ \text{s} < t < 1200$ s. (c) Local magnification of Fig. 3 in the loading period, $1300\ \text{s} < t < 1400$ s.

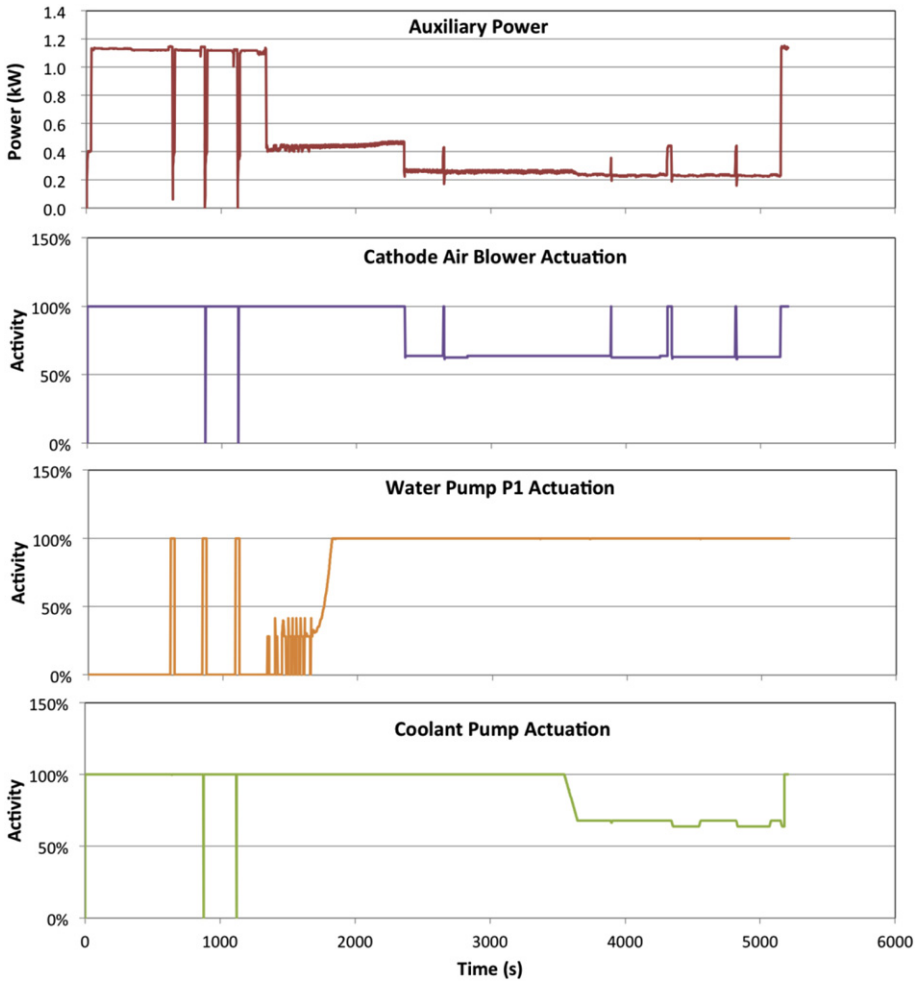

Fig. 6. Relationship of auxiliary power dynamics and the actions of the major auxiliary components.

efficient energy management of the fuel cell CHP generator. That is it should not only cope with strong load variations but also has the ability of maximizing the direct thermal/electrical energy flow from the hydrogen to the load. Specifically, the slave controller I for the thermal recovery system ensures the stack operated within a proper temperature range [33] and recovers the thermal energy efficiently. While, the slave controller II manages the power flow with respect to the energy availability at the DC bus. In general, the controllers

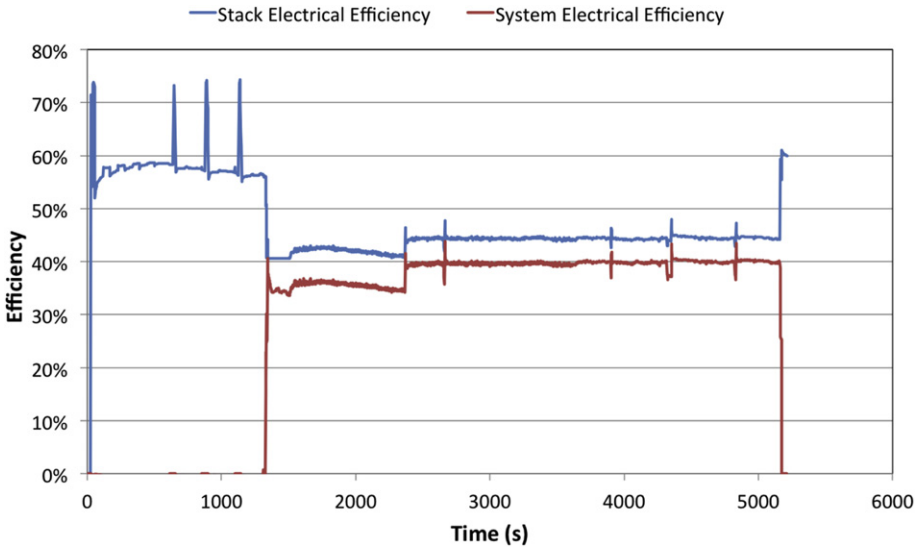

Fig. 7. Comparison of the electrical efficiency of the fuel cell stack and the fuel cell system.

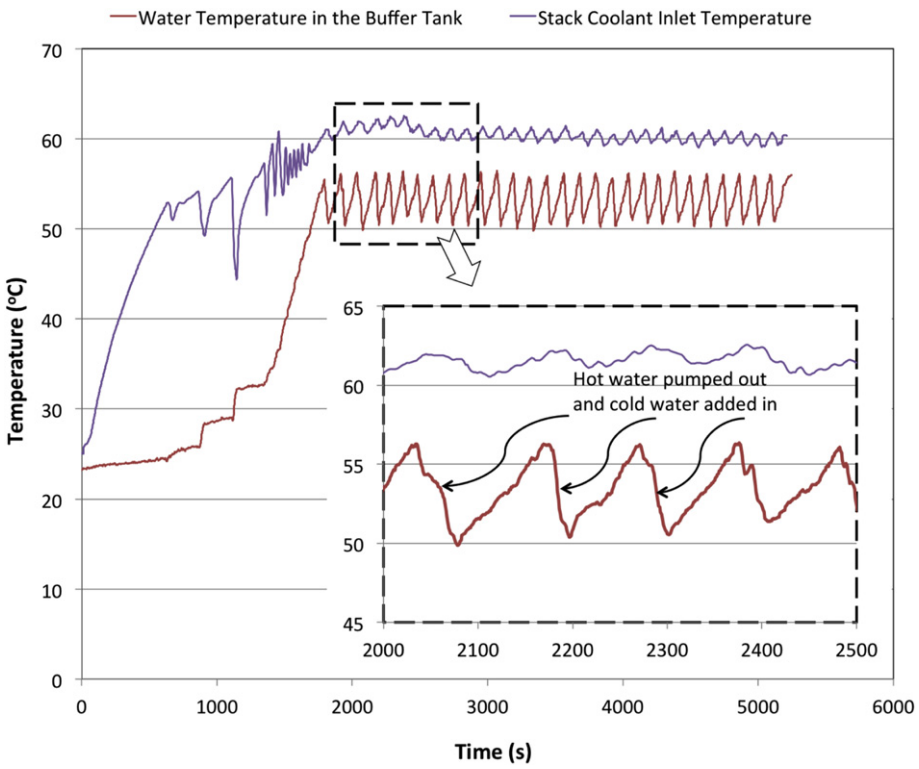

Fig. 8. Distributions of the stack coolant temperature at the stack inlet (SCIT) and the water temperature in the buffer tank (T_b).

divide up the work in monitoring the sensor signals of voltage, current, temperature, pressure, and flow rate in fuel cell CHP generator. These real-time data are recorded and used for decision-making in the control algorithm, in which proper actions are commanded by the controllers to drive actuation devices such as the cathode air blower, solenoid valves, pumps, and relays. All data and parameters in the slave controllers are transferred to the master controller, which are subsequently collected and downloaded to a Notebook through the USB communication port on the master controller. As shown in Fig. 2, a man–machine interface (MMI) is designed to enable real-time monitoring of the experimental data and the operating conditions of the fuel cell CHP generator.

2.5. Experimental conditions

In order to examine the effects of abrupt changes in power demands on the transient electrical/thermal characteristics of the fuel cell CHP generator, a designed external-load profile is given Fig. 3. The external load steps up from zero to 3.2 kW at $t = 1340$ s, then keeps at constant load of 3.2 kW for 3800 s, and finally steps down to zero at $t = 5140$ s. In addition, to further check the reliability and stability of the fuel cell CHP generator, the stack contact is switched off/on purposely to simulate the accidences occurring in operation. As shown in Fig. 3, the stack contact is switched four times during the standby period, i.e., $t = 40$ s, 650 s, 880 s, and

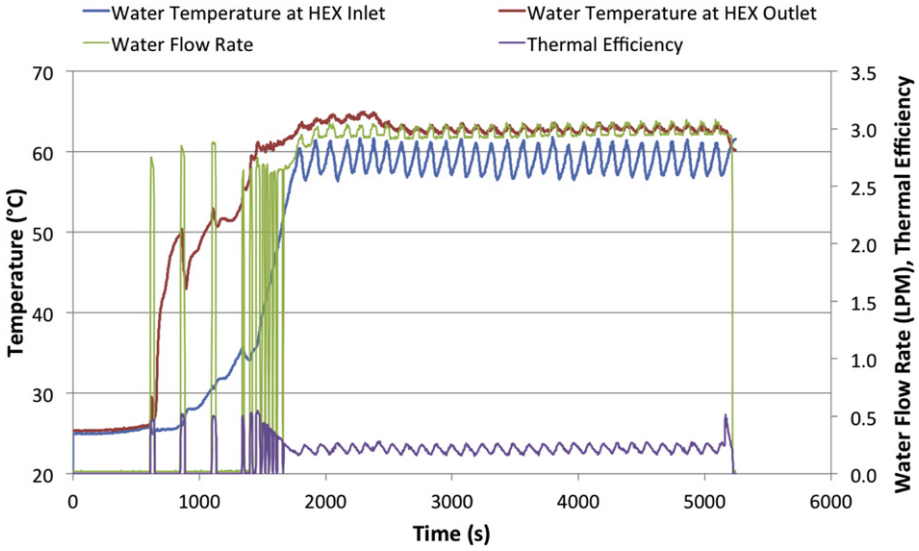

Fig. 9. Distributions of water temperature at the heat exchanger inlet (T_{wi}) and outlet (T_{wo}), water flow rate, and thermal efficiency of the fuel cell CHP generator (ε_t).

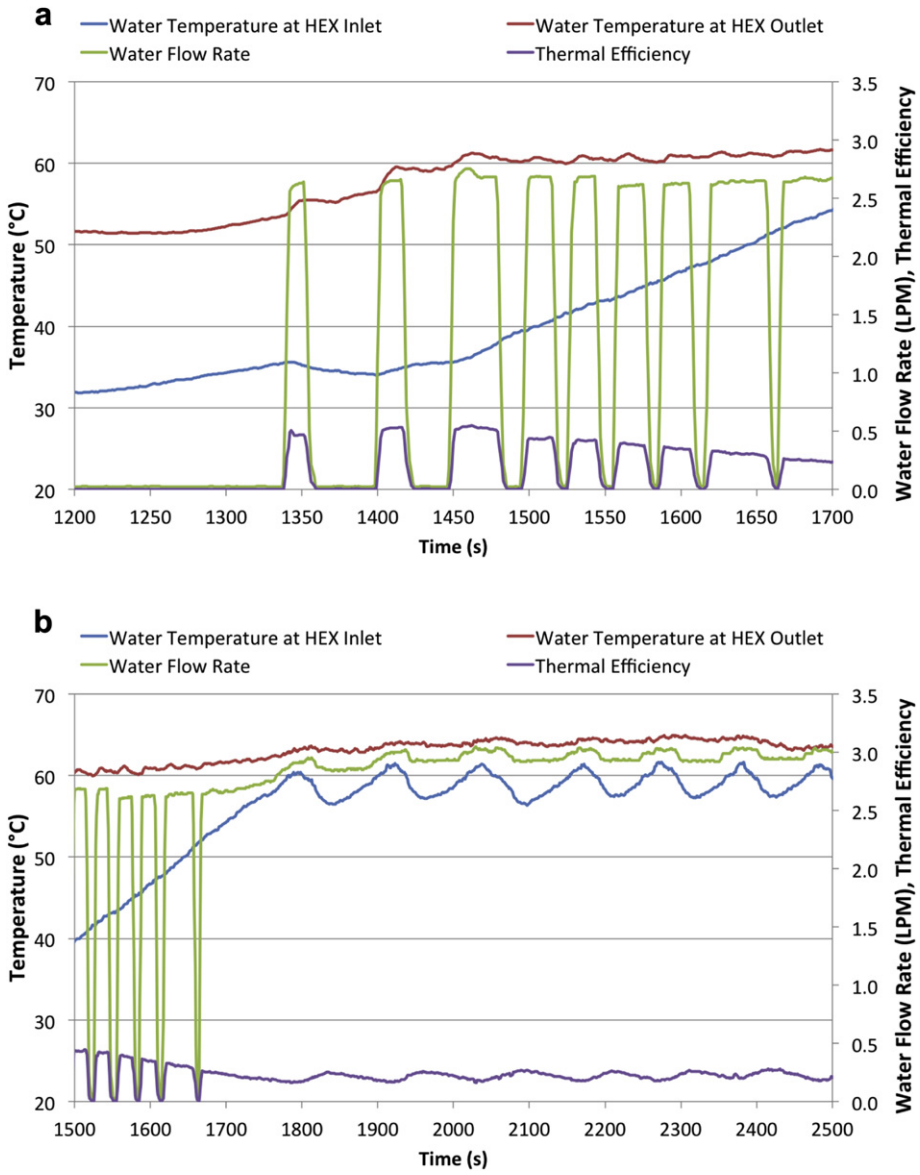

Fig. 10. (a) Local magnification of Fig. 8 around the loading period, 1200 s < t < 1700 s. (b) Local magnification of Fig. 8 in the periodic region, 1500 s < t < 2500 s.

1150 s, respectively. The above external load profile is encoded in a programmable electronic load (Chroma Model 63205), which connects with the DC bus to extract the power from the fuel cell CHP generator.

3. Results and discussion

3.1. Electrical characteristics

Fig. 4 shows the power dynamics of the fuel cell CHP generator under the load profile shown in Fig. 3. A total of four kinds of power are displayed in this figure, i.e., stack power, system power, auxiliary power, and battery power, respectively. It is seen from this figure that the fuel cell stack delivers more than 1.0 kW power to keep the system standby. In addition, to meet 3.2 kW power demand by the external load the fuel cell stack delivers power as high as 3.8 kW. The power discrepancy between the stack and the system represents the combination of the auxiliary power, the battery charge/discharge power, and conversion/transmission losses.

Fig. 5(a)–(c) further shows the local details of Fig. 4 to illustrate the power characteristics of the fuel cell CHP generator. As shown in Fig. 5(a), when the fuel cell CHP generator starts, the battery presides over the auxiliary power for 30 s. That is the battery discharges current to support the auxiliary power. At t = 30 s, the fuel cell stack begins delivering power to supply the auxiliary power. When the stack contact switches off between 40 s < t < 54 s, the fuel cell stack dumps load and the battery takes care of the auxiliary power again. After t > 60 s, the fuel cell stack powers the auxiliary components and charges the battery as well. Fig. 5(b) shows the results between 600 s < t < 1200 s. Clearly, the battery serves as a power deliverer as long as the fuel cell is disconnected from the power conditioning system, which could keep the system in standby; thus avoiding system shutdown. As shown in Fig. 5(c), the stack delivers power to the external load step by step when the system begins powering the external load. Detailed inspection of the figure further has that when the auxiliary power drops sharply from 1.1 kW to 0.4 kW at t = 1345 s, the fuel cell stack keeps its powering trend and delivers the extra power to charge the battery, rather than turns its power down.

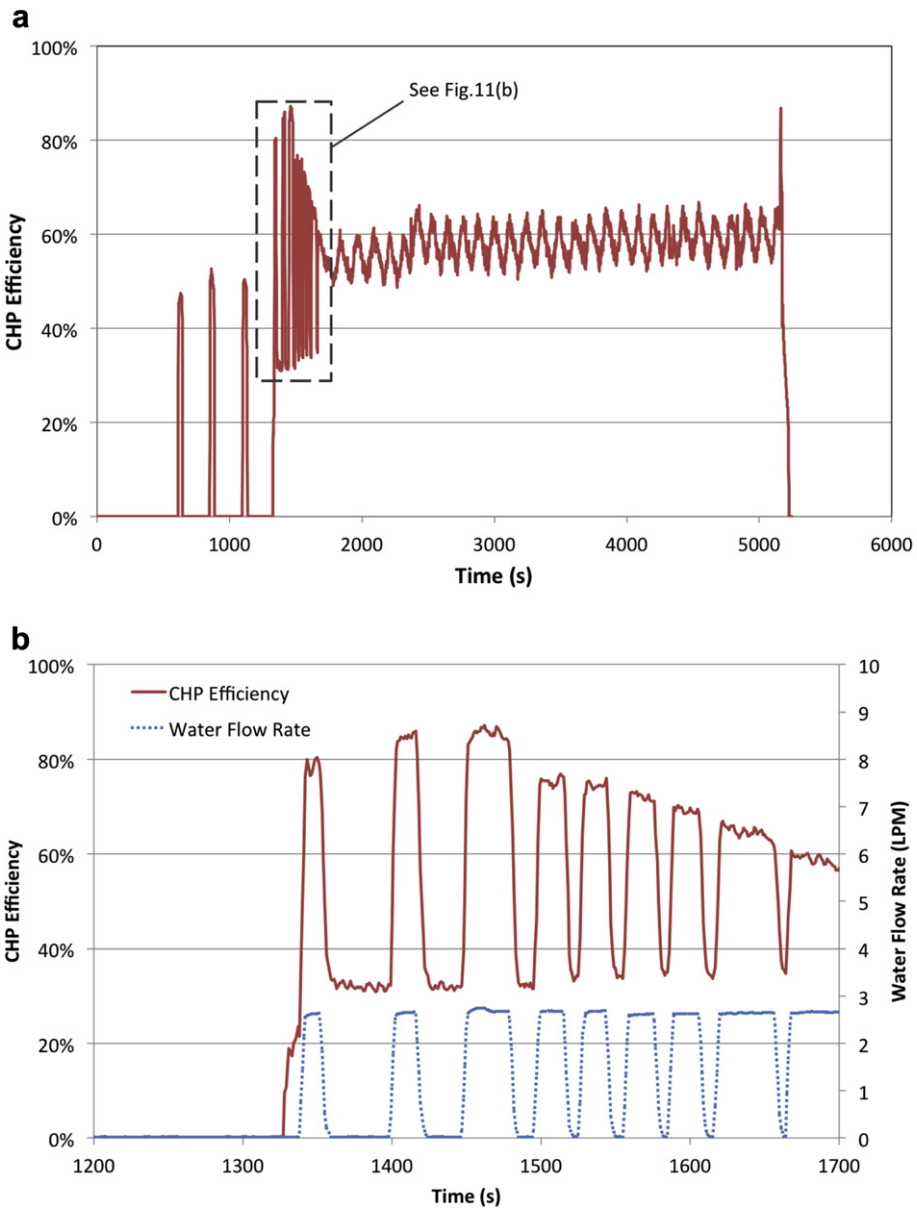

Fig. 11. (a) Transient distribution of CHP efficiency. (b) Transient distribution of CHP efficiency around the loading period, 1200 s $< t <$ 1700 s.

From the results of Figs. 4 and 5, the following conclusion could be made. The hybrid power output from the PEM fuel cell stack and the lithium-ion battery are closely matched with the power demand by the external load as well as the auxiliary power. During the startup period, the power discharged from the lithium-ion battery compensates for the transient inability of the fuel cell stack to provide sufficient power for the system as well as the auxiliary components. In contrast, during the periods of low power demand, the lithium-ion battery stores the extra power provided by the PEM fuel cell stack. Actually, the lithium-ion battery serves as not only the secondary power source to boost the fuel cell system but also an energy buffer to store the energy from the extra power delivering by the fuel cell stack.

Fig. 6 shows the transient distribution of the auxiliary power of the fuel cell CHP generator, which links the activity of major auxiliary components including the cathode air blower, the water pump P1 and, the coolant pump. It is seen from this figure that the dynamics of the auxiliary power is largely correlated with the actuations of these auxiliary components. In general, the main profile of the auxiliary-power distribution is dominated by the actuations of the cathode air blower and the coolant pump, while the little waves distributed on the main profile of the auxiliary power is in consistent with the action of the water pump.

Fig. 7 shows a comparison of the transient distributions of the stack electrical efficiency and the system electrical efficiency. The stack electrical efficiency is defined as the ratio of the gross power delivered by the stack (P_{stack}) to the hydrogen power consumption (P_{H2})

$$\varepsilon_{\text{stack}} = \frac{P_{\text{stack}}}{P_{\text{H2}}} = \frac{I \times V}{n_{\text{H2}} \times \Delta h} \tag{1}$$

where V (V) is the voltage drop across the stack, I (A) is the current through the stack, n_{H2} (mol s^{-1}) is the hydrogen consumption rate, and Δh (kJ mol^{-1}) is the hydrogen enthalpy based on the lower

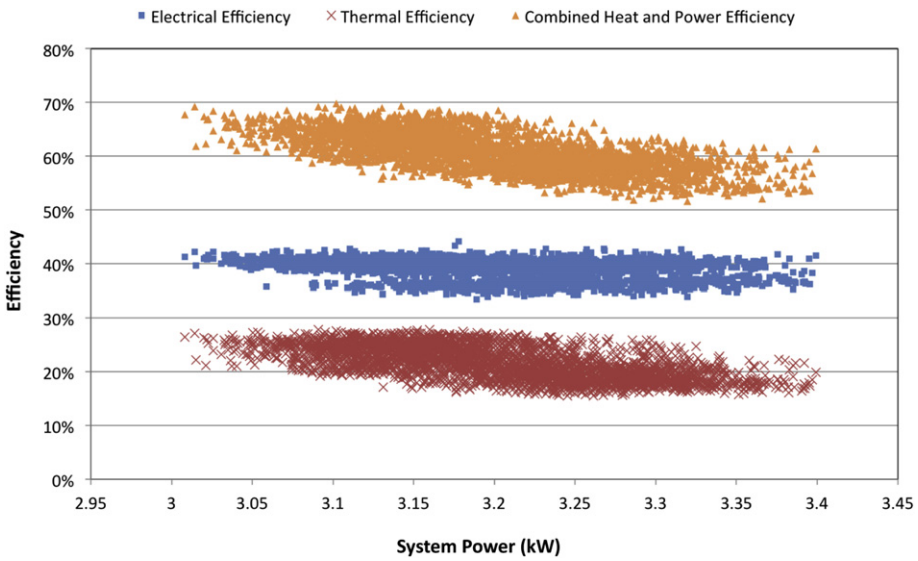

Fig. 12. Scattering of efficiency distributions of the fuel cell CHP generator under the external load around 3.2 kW.

heating value. Similarly, the system electrical efficiency could be expressed as:

$$\varepsilon_e = \frac{P_{system}}{P_{H2}} = \frac{I_L \times V_L}{n_{H2} \times \Delta h} \quad (2)$$

where P_{system} is the net electrical power output to the external load from the fuel cell CHP generator. In contrast to the stack power, it is a direct measure of voltage (V_L) across the external load and the current (I_L) passing through the external load. It is seen from Fig. 7 that the stack electrical efficiency is strongly dependent on the gross power delivered by the fuel cell stack (Fig. 4). It decreases as the gross power extracted from the stack increases. Evidently, the system electrical efficiency is significantly lower than the stack efficiency because a part of the stack power has to support the operation of auxiliary components such as the coolant pump and the cathode air blower. Similar hybrid characteristics were observed in a SOFC system [34]. It is further seen from Fig. 7 that the system electrical efficiency is zero in standby. In addition to the loading at $t = 1340$s, the system electrical efficiency has another step rise at about $t = 2300$s, which is caused by the step drop in the auxiliary power (Fig. 6) due to the actuation of the cathode air blower. Obviously, the system electrical efficiency of the CHP generator is about 35–40% at the constant load of 3.2 kW.

3.2. Thermal characteristics

Fig. 8 shows the transient distributions of the coolant temperature at the stack inlet (SCIT) and the water temperature in the buffer tank (T_b). The former is an important parameter for thermally controlling the fuel cell CHP generator, while the latter represents the degree of thermal energy recovered from the fuel cell CHP generator. As shown in Fig. 8, SCIT increases in standby ($t < 1340$) and is largely fluctuated as the stack contact is being switched and the system is loading. Noteworthy that in the loading period of 2000 s $< t <$ 2500 s the maximum SCIT is about 3 °C higher than the pre-designed value (60 °C). This is because of the delay effect of the water pump. As for the T_b distribution, it increases mildly in standby and then sharply in loading. When it increases higher than T_b>55 °C, the hot water in the buffer tank is pumped to the hot-water reservoir, and simultaneously the cold tap water is added into the buffer tank that maintains the water level in the buffer tank. The water temperature T_b thus drops. As the water temperature T_b reduces lower than 51 °C, the system stops pumping the hot water and closes the tap water; hence T_b rises again. Consequently, the distribution of the water temperature in the buffer tank is varied between $T_b = 53 \pm 3$ °C. This means that the present fuel cell CHP generator is able to provide hot water of over 50 °C for residential use.

Fig. 9 shows the transient distributions of the water temperature at the inlet (T_{wi}) and outlet (T_{wo}) of the heat exchanger, and the water flow rate across the heat exchanger. The corresponding thermal efficiency (ε_t) of the fuel cell CHP generator is also provided. The thermal efficiency ε_t is expressed as the ratio of the rate of the thermal energy (q_w) recovered by the tap water in the heat exchanger to the consumption of hydrogen enthalpy flow, i.e.

$$\varepsilon_t = \frac{q_w}{P_{H2}} = \frac{P_w \times \nu_w \times C_{p,w} \times (T_{wo} - T_{wi})}{P_{H2}} \quad (3)$$

where ν_w ($m^3\ s^{-1}$) is the water volumetric flow rate, ρ_w ($kg\ m^{-3}$) is the water density, and $C_{p,w}$ ($kJ\ kg^{-1}\ K^{-1}$) is the specific heat capacity of water. As noted from the above equation, obviously, the thermal efficiency is subjected to the combined effects of the water temperature difference between the inlet and outlet of the heat exchanger and the water flow rate. In this work, a wheel flow meter (Tokyo Keiso, Model W123) is employed to determine the water flow rate. It measures flow rate of water by counting the number of the built-in wheel's rotation. The sampling rate of the wheel flow meter could reach as high as 10 Hz during the transient measurement. It is seen from Fig. 9 that in the period of 600 s $< t <$ 1300 s T_{wo} increases sharply as the stack contact is switched. Three pulses of the thermal efficiency are coincident with the actuations of the water pump P1, which pumps the water across the heat exchanger with pulse flow. Fig. 10(a) and (b) further gives the local magnifications of Fig. 9 to explain the thermal-fluid characteristics in loading and in the steady state, respectively. Focus is first placed on the water flow rate across the heat exchanger in Fig. 10. Considering the activity of water pump P1 given in Fig. 6 and the results shown in Fig. 10 has that the water pump P1 pumps the water with a pulse mode in loading (1350 s $< t <$ 1700 s) and thereafter with a steady flow rate about 3.0 LPM in the steady state. As for the water

temperature, T_{wi} increases sharply from about 35 °C to about 60 °C in loading (1350 s < t < 1700 s), which subsequently becomes a periodic wavy distribution of an averaged temperature of 57 °C. Clearly, in the loading period of 1350 s < t < 1700 s, the pulse distribution of thermal efficiency ε_t is subjected to the distribution of water flow rate across the heat exchanger. The peaks of ε_t could reach as high as 60%, which are gradually damped due to the reduction in the water temperature difference across the heat exchanger, i.e., T_{wo}–T_{wi}. After t > 1700 s in Fig. 10(b), the distribution of the thermal efficiency is transitioned to a periodic wave with a narrow wavy range of 16%–27%. This means that there is about 16%–27% of hydrogen chemical energy transferred into useful thermal energy by the present fuel cell CHP generator under the constant external load of 3.2 kW.

3.3. Combined heat and power efficiency

In combination of the output electrical power to the external load and the useful thermal energy recovered by water, the combined heat and power efficiency of the present system can be written as

$$\varepsilon_{CHP} = \frac{P_{system} + q_w}{P_{H2}} \quad (4)$$

The CHP efficiency represents the total useful energy provided by the system. Fig. 11(a) shows the transient distribution of CHP efficiency under the external profile of Fig. 3. The local magnification of Fig. 11(a) in the loading period is given in Fig. 11(b). The transient distribution of CHP efficiency in Fig. 11(b) shows a local maximum about 85% in the loading period. In the steady state, as shown in Fig. 11(a), the CHP efficiency ranges from 50% to 67% under the constant load of 3.2 kW. From the dynamic data reported in Fig. 11, the statistics of the system efficiencies in the steady state are further displayed by the function of the system power in Fig. 12. It is clearly seen from this figure that at the system power of 3.2 ± 0.2 kW, the 95% dynamic data of electrical efficiency and thermal efficiency are located at 34–42% (37% in average) and 16–27% (24% in average), respectively. Consequently, 95% of dynamic data of CHP efficiency of the fuel cell CHP generator are distributed in the range of 52%–68% (61% in average).

4. Conclusion

Transient electrical and thermal-fluid characteristics in a PEM fuel cell based CHP generator under step-load conditions have been reported in the present work. The PEM fuel cell based CHP generator is developed by integrating a PEM fuel cell system a power conditioning system, and a thermal recovery system. Imperative efficiency matrices such as stack electrical efficiency, system electrical efficiency, thermal efficiency, and CHP efficiency are provided. Major findings from the measurements of the above transient characteristics of the fuel cell CHP generator are summarized below.

1. Under the severe conditions of abrupt change in the external load, the thermal recovery system is able to recover the thermal energy efficiently in addition to control the stack operation temperature. In addition, the power conditioning system could distribute the power flow that responds to fast change in the external loads.
2. When the system is loading, the thermal efficiency is fluctuated largely and, in contrast, the electrical efficiency is relatively stable, which depends merely on the auxiliary power. The instantaneous CHP efficiency could reach as high as 85% in the loading period.
3. With about 55% in system power capacity (3.2 kW in 5.8 kW), the present fuel cell CHP generator has an average electrical efficiency about 37% and an average thermal efficiency about 24% Consequently, the CHP efficiency could reach 61% in average.

Acknowledgments

The author professor Jenn Jiang Hwang would like to thank the National Science Council of Taiwan, for financially supporting this research under contract no. NSC 98-2221-E-024-015-MY2.

References

[1] ASHRAE Handbook HVAC Systems and Equipment, ASHRAE Inc., USA, 2000.
[2] T. Brenscheidt, J. Janowitz, H.J. Salge, H. Wendt, F. Brammer, Int. J. Hydrogen Energy 23 (1998) 53–56.
[3] Q. Okada, K. Yokoyama, Fuel Cells 1 (2001) 72–77.
[4] The DoD residential PEM fuel cell demonstration program, Fuel Cells Bull. 2003 (2003) 11–13.
[5] J.J. Hwang, M.L. Zou, Int. J. Hydrogen Energy 35 (2010) 8644–8653.
[6] J.J. Hwang, M.L. Zou, J. Power Sources 195 (2010) 2579–2585.
[7] P. Costamagna, S. Srinivasan, J. Power Sources 102 (2001) 242–252.
[8] W.M. Ellis, M.B. Gunes, ASHRAE Trans. (2002) 108–111.
[9] K. Krist, J.D. Wright, Solid Oxide Fuel Cell Residential Cogeneration, 1999 Joint DOE/EPRI/GRI FC Technology Review Conference, Chicago, USA, 1999.
[10] New Energy Foundation, Report data from the Large Scale Residential Fuel Cell Demonstration Project in 2008. URL: http://happyfc.nef.or.jp/pdf/20fc.pdf (in Japanese).
[11] D. Carter, Fuel cell residential micro-CHP developments in Japan, Analyst Views Fuel Cell Today 29 Feb 2012.
[12] Osaka Gas, ENE-FARM Product Information, htttp://home.osakagas.co.jp/search_buy/enefarm/(in Japanese) (retrieved in August 2012).
[13] Toshiba Fuel Cell Power Systems Corporation, ENE-FARM Specifications, http://www.toshiba.co.jp/product/fc/products/pdf/catalog6.pdf (in Japanese) (retrieved in August 2012).
[14] Tokyo Gas Co., http://home.tokyo-gas.co.jp/enefarm_special/index.html (in Japanese) (retrieved in August 2012).
[15] Japanese Group Unveils SOFC Ene-Farm Residential Cogen Unit, Fuel Cells Bull. 2012 (2012) 4.
[16] W. Collella, J. Power Sources 106 (2002) 388–396.
[17] J.J. Hwang, D.Y. Lai, J. Power Sources 143 (2005) 75–83.
[18] A. Ferguson, V.I. Ugursal, J. Power Sources 137 (2004) 30–42.
[19] G. Gigliucci, L. Petruzzi, E. Cerelli, A. Garzisi, A. La Mendola, J. Power Sources 131 (2004) 62–68.
[20] P. König, A. Weber, N. Lewald, T. Aicher, L. Jörissen, E. Ivers-Tiffée, et al., J. Power Sources 145 (2005) 327–335.
[21] S. Obara, Int. J. Hydrogen Energy 31 (2006) 1807–1818.
[22] M. Radulescu, O. Lottin, M. Feidt, C. Lombard, D. Le Noc, S. Le Doze, J. Power Sources 159 (2006) 1142–1146.
[23] S. Campanari, E. Macchi, G. Manzolin, Int. J. Hydrogen Energy 33 (2008) 1361–1373.
[24] J.J. Hwang, P.C. Wang, J.K. Kuo, Fuel Cells 12 (2012) 326–333.
[25] A.D. Hawkes, D.J.L. Brett, N.P. Brandon, Int. J. Hydrogen Energy 34 (2009) 9545–9557.
[26] N. Briguglio, M. Ferraro, G. Brunaccini, V. Antonucci, Int. J. Hydrogen Energy 36 (2011) 8023–8029.
[27] K. Maeda, K. Masumoto, A. Hayano, J. Power Sources 195 (2010) 3779–3784.
[28] W.R. Chang, J.J. Hwang, F.B. Weng, A. Su, J. Power Sources 166 (2007) 149–154.
[29] J.J. Hwang, D.Y. Wang, N.J. Shih, J. Power Source 141 (2005) 108–115.
[30] Mindman Industrial Co. Ltd., http://www.mindman.com.tw/upload/prod_download/C_MSUS.pdf (in Chinese) (retrieved in September 2012).
[31] J.J. Hwang, J. Electrochem. Soc. 153 (2006) A216–A224.
[32] J.J. Hwang, P.Y. Chen, Int. J. Heat Mass Transfer 49 (2006) 2315–2327.
[33] J.J. Hwang, C.H. Chao, Int. J. Hydrogen Energy 32 (2007) 405–414.
[34] P. Costamagna, L. Magistri, A.F. Massardo, J. Power Sources 96 (2001) 352–368.